

Technical Paper

Function-aware slicing using principal stress line for toolpath planning in additive manufacturing



Eder Sales ^a, Tsz-Ho Kwok ^{a,*}, Yong Chen ^b

^a Department of Mechanical, Industrial and Aerospace Engineering, Concordia University, Montreal, QC H3G 1M8, Canada

^b Epstein Department of Industrial and Systems Engineering, University of Southern California, Los Angeles, CA 90089, United States

ARTICLE INFO

Keywords:

Slicing
Toolpath planning
Additive manufacturing
Principal stress
Topology optimization

ABSTRACT

Additive manufacturing (AM) has been widely used in many different areas due to its unique advantages, such as the possibility of creating complex shapes, no specific tools required, relatively fast, and less material waste with light-weight designs. The design freedom enabled by AM also allows a component to be highly optimized on its topology and shape according to its function. Currently, there are advanced algorithms that enable designers to perform topology optimization (TO) in the computer-aided design (CAD) phase. However, the optimization results are not considered during the downstream AM process planning like toolpath generation, and the optimized structure may lose its designed performance. Instead of only considering TO in the CAD phase, this work presents a breakthrough in adopting the TO principles in the toolpath planning process and considering the toolpath characteristics presented in the AM processes. Since toolpaths are lines, this paper applies a line-based TO method that uses the principal stress line (PSL) as guidances to the generation of toolpaths to improve structural rigidity. The PSL-based method is efficient, controllable, and able to consider the characteristics of the AM process. The computation results can be directly converted into toolpaths that can be faithfully fabricated and achieve the component function specified in the design phase. Structural tests were performed on the developed method. The experimented results demonstrate that the strategy of applying the PSL-based toolpath planning is a promising direction to incorporate topology optimization from the CAD phase to computer-aided manufacturing (CAM). To the best of our knowledge, this study is the first to explore the use of PSL in the AM's toolpath planning.

1. Introduction

Toolpath planning is important for additive manufacturing (AM) processes [1], such as fused filament fabrication (FFF). Until today, a computer-aided design (CAD) model is first converted to a geometric file like a set of triangular meshes (e.g., STL file). The model is then processed by a toolpath planning software system to generate motion control instructions that can be used by an AM printer [2]. Since most AM processes accumulate material layer-by-layer, the toolpath planning software needs to slice the three-dimensional (3D) geometry into multiple two-dimensional (2D) layers, mainly based on geometrical information of the CAD model without considering its designed function. Each layer can then be formed by depositing material on the layer boundary, followed by constructing an internal structure known as the infill of the interior area. The infill is responsible for increasing the component strength and also works as a support structure for the upper

layers. The infill can be defined as a percentage of the filled volume, in which 100% infill means that the component is fully filled. Different combinations of infill patterns and percentages can be selected to reduce the weight and fabrication time [3,4].

Research shows that appropriate construction of filling patterns can improve parts for their intended function as well as part quality and print efficiency [5–8]. The AM technology can fabricate components with better quality for a broader range of applications if suitable infills for the 3D printed layers are used based on functional design requirements [9]. To fully utilize the capability of AM, several optimization tools have been developed for structures as well as the infill [10]. However, how to incorporate the design function in the slicing of a CAD model so the planned toolpath can lead to a 3D printed part with optimized performance is still an open question.

Modern CAD software can perform optimization on size, shape, and topology based on required design functions [11,12]. Size and shape

* Corresponding author.

E-mail address: tszho.kwok@concordia.ca (T.-H. Kwok).

optimization find the optimal size of elements and the location of nodes for a given structure, while topology optimization (TO) optimizes material distribution within a given domain. The inputs of such design methods are typically applied loads and boundary constraints. TO can generate an optimized design for 3D printed parts considering both functional and geometrical constraints and objectives, maximizing design functions such as stiffness. Some can also consider anisotropic material properties during the optimization [13,14]. TO algorithms have been successfully implemented in modern CAD software. However, typical TO methods are computationally expensive and mainly done in the CAD phase. The optimized results need to be saved as a CAD model and transferred to the AM system for toolpath planning. Hence, even TO has generated an optimized CAD model considering the design function (Fig. 1(a) and (b)), the generated toolpath may lead to a 3D printed part with inferior performance. For example, while FFF can fabricate complex geometries obtained via TO, the final toolpath used to produce the designed part is determined by a slicer that does not consider the design function of the part (Fig. 1(c)). If the toolpath does not corroborate with the TO results, it will limit or even reduce the structural strength of the TO design obtained in the CAD phase. As an illustration, assume the TO result from the CAD phase is a vertical bar to support axial loads. Without knowing the design requirement, the slicer would generate an arbitrary toolpath formed by horizontal lines perpendicular to the load. This is one of the worst cases because the load needs to be held by the adhesive strength between the lines, which is much weaker than the material strength. Besides, typical TO methods do not consider manufacturing parameters and produce an output with a limited resolution, which cannot be directly used for process planning.

These observations motivate our research that aims to connect the TO results with the slicing operations such that the manufacturing results respect the structural properties defined in the design phase. Our goal is to apply the TO principles in the toolpath planning to maintain the imposed functional requirements defined for a part. Nevertheless, there are a few challenges that need to be addressed to realize this objective. First, TO is usually a computationally expensive process (at least a few minutes), and if it is applied to every single layer in the slicing, an unrealistic long time will be required for process planning. Second, the TO results are generally discretized (e.g., pixels), but the toolpaths of FFF are a set of lines, so the conversion between them is required. Furthermore, if a coarse discretized domain is used to achieve a higher speed, the TO results will be in low-resolution, and the conversion into toolpath will be more unreliable.

The objective of this paper is to apply the PSL method from topology optimization to the generation of toolpaths for additive manufacturing. Although the idea of using PSL is not new, the previous works were mainly about mechanics and geometry, and they did not consider planning and fabrication-related issues. There is a missing gap, and the same idea presented by previous works cannot be directly applied to toolpath planning. For example, in the traditional method, finite element analysis (FEA) is commonly needed to optimize a structure. However, performing FEA to generate a toolpath in every single layer takes a tremendous amount of time. It is unknown that how optimization

can be applied in toolpath planning without the high computational cost. In addition, since the PSLs are not some uniform lines, it was unknown that how to print the lines when there are collisions and how to satisfy a given infill ratio, just to name a few. These are some research questions of this research, and the contributions of this paper come from answering them to generate new knowledge, including:

- By inputting a strain field with the CAD model to the slicer, the stress values can be recovered in each layer, so that the PSL method can be applied to toolpath planning and structurally strong toolpaths can be generated efficiently.
- With the help of the recovered stress field, a classification on tensile and compression was performed on the PSLs, so the planned toolpath can be printed in proper order in case of intersections to preserve the structural integrity.
- As a non-uniform infill pattern, its mapping to the infill ratio is not defined. Therefore, a binary search method is developed to find the optimal density of PSLs such that the desired infill ratio can be achieved.
- The relationship between the extrusion rate and the line width is studied. Based on it, the extrusion rate can be controlled to minimize excessive materials caused by overlapping toolpaths.

Experimental results show that the developed PSL-based slicing method is promising for AM toolpath planning with significant advantages on efficiency and printability. Physical test results demonstrate that the optimized toolpath can redistribute the stresses during fracture while uniform infills have the stresses that concentrate in the same regions. A destructive test was also performed, which showed a 50% improvement in mechanical strength using the same amount of material.

The rest of the paper is organized as follows. Related works are reviewed in Section 2. An overview of the PSL-based toolpath planning method is presented in Section 3. Section 4 discusses the technical details when applying PSL in slicing with the considerations of additive manufacturing. The experimental results are presented in Section 5, and a discussion on possible variations of the method is presented in Section 6. After that, the paper is concluded in Section 7.

2. Related work

The presented work is related to topology optimization and infill generation. This section is going to review these two areas.

During the component design in the CAD phase, topology optimization can be applied to reduce material usage while still satisfying the required design objective. Different TO methods have been developed, such as Level Set, Solid Isotropic Material Penalization (SIMP), and Ground Structure. The level set method was presented by Osher and Sethian [15] by following fronts propagating with the curvature-dependent speed. Allaire et al. [16] coupled level set with a topological derivative to develop an algorithm for TO. Suresh and Takalloozadeh [17] developed a stress-constrained TO. Mirzendehdel et al. [14] proposed a strength-based TO using the non-homogeneous

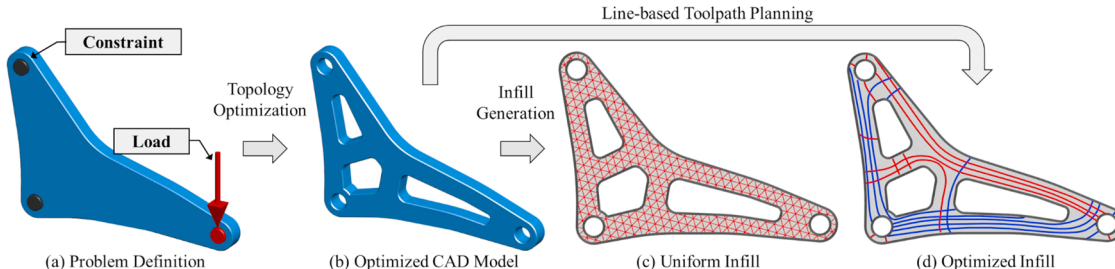


Fig. 1. When topology optimization is only applied in the CAD model, the generated infill pattern during slicing may not reflect its structural properties. This paper proposes a line-based toolpath planning using principal stress line (PSL) to generate optimized infill toolpaths for fabrication.

failure criteria (such as Tsai-Wu), which shows an improvement in the maximum supported load when compared with the von Mises yield criterion-based results. Xia et al. [18] used the level set to solve the shape and topology optimization problem to minimize the global measure of stress. A MATLAB code to run the level-set TO is available online [19]. SIMP [12,20] is another popular TO strategy [21]. SIMP's basic principle is to execute a finite element analysis (FEA) and then run an optimization of the material density for all the elements inside the design domain. This process is repeated until the convergence is reached. A third type of TO method is the Ground Structure (GS), which was proposed by Dorn [22] and is largely used in the design of trusses. Since the initial GS algorithms only allowed the removal of bars, a high-density initial structure was necessary to obtain good optimization results. To overcome this limitation, Hagishita and Ohsaki [23] proposed an algorithm to allow both adding and removing bars. In addition, there are hybrid TO methods. For example, Zegard and Paulino [24] use both SIMP and GS methods to obtain optimal structural mechanisms for AM.

In the context of the infill generation in AM, different methods have been developed to optimize the infill of a component. Adaptive centroidal Voronoi tessellation was used to create a pore-based internal structure, and a strength-to-weight optimization was performed to obtain the minimum internal structure that can support a specific load [5]. Wu et al. [10] considered a bone-like optimized infill structure to maximize the mechanical stiffness using the voxel-wise topology optimization. An infill generated by the optimization of the global stiffness under any load distribution was proposed by Wang et al. [6] based on the saddle point algorithm. Truss-like cellular structures can also be optimized using the density information [25,26]. Ezair et al. [27] used a slicing approach to generate print-paths in any desired 3D direction, using a trivariate model and a directional field as the input. The experimental examples were printed using a simple 3-axis 3D printer. Jin et al. [28] performed a study on curved layer fused deposition, and developed a physical model with slicing procedure and path generation algorithms to allow the fabrication of curved surfaces with continuous lines. Wu et al. [29] proposed a method to create infill structures on rhombic cells. Liu et al. [30] introduced a methodology to produce hybrid infill patterns based on the level set principle. Void parts of the structure, under low stress, were filled with non-optimized patterns. Numerical examples were given in their study; however, no physical tests were performed to demonstrate the mechanical strength of the obtained infill design. Steuben et al. [31] proposed an implicit slicing algorithm, in which the generated toolpath was based on level sets of arbitrary heuristic-based or physics-based fields. In their application, they use von Mises to obtain the toolpaths. The von Mises stress is calculated from the Cauchy stress tensor, mostly used as a failure criterion. This is because the stress tensor is encapsulated into one scalar value, which can then be compared with the yield strength of a material to predict its yielding under complex external loads. Using one single scalar value for stress measurement is easy and user-friendly, but some critical information is lost. Since the scalar values of von Mises do not give a direction, the toolpath is generated by isolines (the contour is created connecting the points with the same value). Although in their results, the regions with high-stress concentration are denser than those with low-stress areas, the output toolpaths do not intersect due to the homogeneous continuum response. This lack of connection can affect the performance of the final fabricated component. Furthermore, from Michell's theorem [32], a minimum weight structure needs to satisfy the condition that the strains distribute along with the structure members. That is, the material should lie along the lines of the principal strain such that they are fully loaded. This motivates us to apply the principal stresses rather than the von Mises stress. The principal stresses have both the stress values and the principal directions. Therefore, it is possible to trace continuum lines inside the infill domain.

The aforementioned works are well established for topology optimization and infill generation, by focusing mainly on the part geometry

and the shape of the infill pattern. However, they do not take into consideration the properties of the toolpath-based AM processes. For example, the widely used FFF process [2] produces parts with anisotropic characteristics, demonstrated by the low mechanical property of a component when the load is applied perpendicularly to the filament orientation [7,33,34]. Similar results were obtained by Koch et al. [35], in which orientation, solidity, and edge effects were studied. Wittbrodt and Pearce [36] even found out that the filament pigment color could affect the component mechanical strength. These studies demonstrate there is an influence of the filament orientation and conditions in the final component strength. Therefore, the toolpath planning in the AM process should consider both design and manufacturing requirements.

Recently, PSL has been utilized in various applications. An important characteristic of PSL is that it is computationally fast. Hence, a PSL-based method allows good interaction between the user and the design interface, since the optimization result can be computed in real-time. Daynes et al. [37] used isostatic lines to optimize functionally grade lattice structures. They employed a commercial finite element solver to perform topology optimization and obtained the core density to generate cell geometry. Size optimization (using the same finite element solver) was also used to resize the cross-sectional diameters of the structures. Gao et al. [38] presented an effective method to generate ground structures by adding nodal points at the intersection of principal stress trajectories. Tam and Mueller [39] demonstrated the use of principal stress lines to deposit filament along the stress lines of the component. Using a six-axis robot arm, they were able to produce curved 3D surfaces directly. A PSL-based topology optimization method was also presented by Kwok et al. [40]. Their work demonstrates a good correlation with other topology optimization methods, as presented by Andreassen et al. [41]. Although PSL-based optimization is performed in those frameworks, they are all based on the CAD model and did not consider the toolpath planning and fabrication characteristics. Therefore, since there is no connection between the CAD and CAM phases, the component performance can be reduced as the manufacturing process is not considered. Differently, this paper aims to apply the PSL-based toolpath planning in the two-dimensional (2D) slicing, such that the generated toolpaths consider the manufacturing characteristics (FFF in our study) and are optimized for the design function as well.

3. Overview

As mentioned before, the majority of structural optimization is done in the CAD phase. However, since the layer-based AM processes have anisotropic characteristics, the printed part's final property is also determined by the layout of the toolpath used in fabrication. This work proposes a function-aware toolpath planning method by applying the topology optimization principle in the layer slicing operation. To achieve this goal, the design function-based slicing method must be fast, considering manufacturing parameters, and converting the part design results to machine instructions seamlessly. Since a toolpath is a set of lines in AM processes such as FFF and direct energy deposition (DED), it is preferred to employ a line-based topology optimization method to the toolpath planning for AM. Recently, some TO research focuses on putting the material to experience only the principal stresses (i.e., no shear stress), since the shear modulus usually is smaller than the Young's modulus. This can be achieved by placing the material along the principal stress line (PSL), which can be traced on a stress field. PSL can be computed efficiently, and more importantly, it is represented in lines that can be directly used as the toolpaths. Therefore, the PSL can be directly applied in the toolpath planning for AM, which takes not only the design information but also the additive manufacturing properties into account. Based on our knowledge, this study is the first to explore the use of PSL in AM toolpath planning.

For the conventional TO methods, the applied loads, boundary conditions, and the structural information of the part are specified, and then an FEA is performed to compute the material distribution.

However, applying the TO principle to toolpath generation means that the computationally expensive FEA needs to be done in each layer. In addition, all the design information needs to be inputted into the slicer. In our method, only a strain field needs to be passed into the slicer without any additional design information. Given the strain field, the stresses can be recovered instantly at every point inside the domain, and the principal stresses can be computed efficiently for each layer to draw the PSLs. The strain field can be represented by the strain values specified on each vertex and inputted into the slicing system using a common 3D printer file format (e.g., AMF, 3MF, OBJ). Therefore, the overall pipeline of the framework is as follows, with only minor changes to the current AM data preparation pipeline (as illustrated in Fig. 2):

1. With the defined loading conditions, the FEA is applied to a CAD model to compute a 3D stress field.
2. The CAD model, together with the stress field, is saved as a mesh file and passed into the slicing software.
3. The model is sliced into a set of 2D planes, and the 3D stress field is mapped onto the sliced planes to generate 2D stress fields in each layer.
4. Within each 2D plane that requires infills, PSLs are traced on the 2D stress field with the consideration of the manufacturing requirements.
5. From the PSLs, the output will be the toolpaths (G-code) that can be directly fed to the AM machine for the fabrication of the CAD model.

The FEA in step 1 can be performed using commercial CAD tools in which the model is designed, and the stress field in step 2 can be saved in the AMF format. The stress field can be represented by the strain values specified on each vertex and inputted into the slicing system. Since the AMF format can support the specification of textures or materials, the strain values in x -, y -, and z -axes can be stored as the r , g , and b colors, respectively. An example is shown in Fig. 3, where the coordinates of a vertex are stored in $\langle x \rangle$, $\langle y \rangle$, and $\langle z \rangle$, while the strain values of the same vertex are stored in $\langle r \rangle$, $\langle g \rangle$, and $\langle b \rangle$. The strain values at the vertices are used to recover the principal stresses at any locations within the elements. In step 3, we apply a method similar to the one used by Steuben et al. [31], mapping the 3D stress field to the 2D ones by eliminating the stresses in the z -direction. The difference is that they used the von Mises stresses, while this work uses the principal stresses. Given a desired infill ratio, the infill is constructed in step 4 using PSLs. Since non-uniform infills are meant for the 2D planes that require hatching, if there are 2D planes or portions of them that require full coverage (e.g., top and

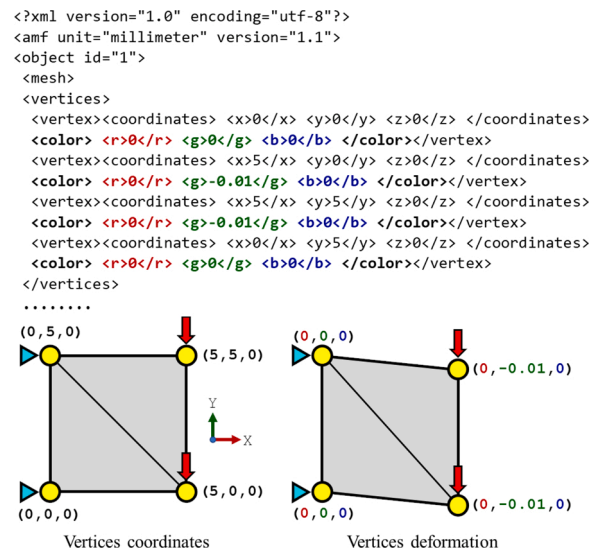


Fig. 3. AMF format example illustrating a mesh and a strain field. The strain values are stored as the r , g , and b colors of each vertex.

bottom surfaces), the traditional uniform toolpaths can be used. The PSLs are a set of lines represented by ordered points, so they can be efficiently converted to the machine code point-by-point in step 5.

It is worthwhile to mention that the 2D projection of the stress field in step 3 was based on the nature of most 3D printing technologies that accumulate material using the layer-based approach. Since the physical process is done by 2D layering, the structural integrity of the printed object is also only as good as the planned 2D structures. As an early attempt to optimize toolpath for structural consideration, this paper has an assumption that the principal stress directions are mostly in-plane. It is also worth mentioning that this work is complementary to 3D topology optimization. As most AM processes fabricate parts layer-by-layer, even the part is topologically optimized in 3D, the toolpath planning in every single 2D layer is still needed to achieve the best structural property.

Among all the steps, step 4 is the most challenging part and will be the main focus of this paper. To facilitate the explanation in detail, the strain field is assumed to be given as the input, and the concept is demonstrated in various examples where the toolpath planning is performed via slicing operation of a specific domain in multiple 2D layers.

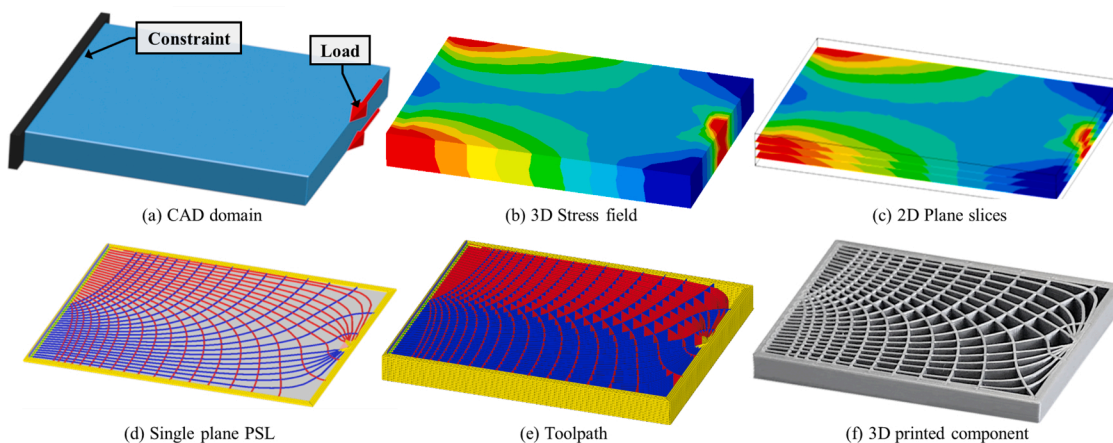


Fig. 2. The framework overview for applying the line-based TO method in the toolpath planning. (a) The initial domain-containing boundaries conditions and loads. (b) The CAD model and the related stress field are inputted into the AM system. (c) The model is sliced, and the stress field is mapped onto each 2D plane. (d) The PSLs are generated in one single layer based on the input 2D stress field. The walls are colored in yellow. Red and blue indicate tensile and compressive PSLs, respectively. (e) The PSLs can be readily converted to toolpaths as well as G-code for fabrication. (f) The 3D printed part. (For interpretation of the references to color in this figure legend, the reader is referred to the web version of this article.)

As a proof-of-concept, the method has been implemented for an FFF printer, but the framework could be used by other toolpath-based AM processes as well. Before giving the technical details of applying PSL for toolpath planning, the fundamental of PSL is presented.

3.1. Principal stress line (PSL)

Given a domain $\Omega \in \mathbb{R}^2$ and a stress field, it is possible to obtain the stress tensor

$$\sigma = \begin{bmatrix} \sigma_{xx} & \tau_{xy} \\ \tau_{xy} & \sigma_{yy} \end{bmatrix}$$

where σ_{xx} , σ_{yy} and τ_{xy} are the stress components. The tensor defines the state of stress at a point $p_i \in \Omega$ and consequently, the principal stress for any specific point p_i can be obtained by

$$\sigma_{1,2} = \frac{1}{2} \left(\sigma_{xx} + \sigma_{yy} \pm \sqrt{(\sigma_{xx} - \sigma_{yy})^2 + 4\tau_{xy}^2} \right) \quad (1)$$

where σ_1 is the maximum principal stress, and σ_2 is the minimum principal stress. The principal direction θ_i of point p_i can be calculated by

$$\tan(2\theta_i) = \frac{2\tau_{xy}}{\sigma_{xx} - \sigma_{yy}}, \quad (2)$$

Hence, the principal stress line (PSL) is a line in which all segments are along with the principal stress directions. In our study, the PSL starts from a seed point p_0 within the domain, the PSL can be traced by iteratively moving a small step along the principal direction until it exits the domain, and every subsequent point can be calculated using

$$p_{i+1} = p_i + \Delta \cdot v(\theta_i), \quad (3)$$

where $v(\theta_i)$ is a unit vector aligned with the principal angle θ_i and Δ is the increment size parameter. In this study, it was used $\Delta = 0.1$ mm. This value was determined considering the finite element mesh size and the 3D printer precision characteristics. As there are two principal directions at each point, the one closest to the previous angle θ_{i-1} would be selected.

However, as it can be observed in Eq. (2), when σ_{xx} and σ_{yy} are equal, the principal direction is undefined. Kowk et al. [40] used a strategy based on the optimal regions to make sure the structure is always generated in the well-defined regions. The optimal regions are classified into five types according to σ_1 and σ_2 . Here we grouped them in three because of the symmetry in positive and negative values:

$$\begin{aligned} R : |\sigma_1| > 0 \text{ and } \sigma_2 = 0 \\ S : \sigma_1 = \sigma_2 \\ T : \sigma_1 > 0 \text{ and } \sigma_2 < 0 \end{aligned}$$

Normally, the stresses would not be exactly zero, so $\sigma = 0$ commonly means that it is not significant, e.g., its value is close to zero or very small when compared to the other principal stress. In different regions, the stresses could run in only one direction (R), two directions (T), or all directions (S). The well-defined region is the T region. More details could be found in the previous work [40].

3.2. PSL-based toolpath

The previous work [40] used PSLs to generate a truss structure, which only requires a few PSLs to construct the trusses with their intersections as the joints. On the one hand, the requirement of PSLs in the previous work is not high. Even if there are irregular PSLs (e.g., caused by round-off errors and mismatch in angles at the region transitions), they can simply discard these PSLs and use other close ones that are regular. On the other hand, they choose the subdivision points based on the curvature of PSLs, the sampling is basically very coarse, and there is barely interference between lines. However, the PSLs requirement is

much higher in the toolpath planning because every segment of the PSLs will be directly converted into the final toolpaths. In addition, infill patterns are preferred to be uniform so that the part is close to isotropic and can avoid vulnerable points that may cause the part to collapse when an unexpected load is applied. Meanwhile, to optimize a structure, more materials should be distributed in high-stress areas. These two objectives, uniformity and mass redistribution, sound contradicting. Our work tries to make a balance between them. First, by uniformly sampling the seed points on the domain boundary, it makes sure that the whole surface of the part is supported by some deposited materials. Second, the PSL is applied to achieve different material densities throughout the domain due to the PSL's trajectory, fulfilling the target infill ratio. Because of the much denser coverage, the interference between the lines is not negligible and must be dealt with during the toolpath planning. Therefore, although the previous work [40] and this paper share the same starting point, the objectives and the methodology are very different. The PSLs computed in the previous work did not consider the infill properties and cannot be directly used as toolpath. The unique developments in this paper are presented in the following and the coming sections.

To make sure the computed PSLs are smooth, the tracing should consider not only the previous angle but also the optimal regions presented in Section 3.1. Therefore, different strategies need to be used in different regions. The T region is the region with two well defined principal directions perpendicular to each other. The tracing in the T region is the same as Eq. (3) where the angle closer to θ_{i-1} is selected as θ_i . For the R region, there is only one principal direction, but indiscriminately using it as θ_i might result in a sharp turn for the PSL. This kind of PSL is not structurally sound, so we treat the R region using the same way as the T region, by adding another direction which is 90° different from the principal direction as the second principal direction. The S region does not allow the use of Eq. (2) to obtain the principal directions since σ_{xx} and σ_{yy} are equal or very close. In this case, θ_i becomes undefined, and any direction would be a valid direction. Therefore, the previous direction θ_{i-1} is used to calculate the next point p_{i+1} .

The projected 2D stress field is usually smooth, and the difference between the current and the previous angles is usually small, i.e., $\theta_{i-1} \approx \theta_i$. However, if there is field discontinuity within a layer, it can create a significant angle difference between two consecutive points, resulting in irregular PSLs with sharp features. In these cases, the tracing of a PSL should preserve the PSL's smoothness as a priority. Specifically, if the angle difference between two points is larger than a certain threshold ($|\theta_{i-1} - \theta_i| > \theta_{\max}$), the previous direction is maintained to avoid any sharp turns in a PSL. A value of 30 degrees is used for θ_{\max} in this paper.

The new tracing strategy and the use of different optimal regions can generate smooth PSLs; however, some PSLs might not have structural meaning. For example, a PSL is too small to be printed (e.g., a line that is smaller than the nozzle diameter), or it is a duplicated line (e.g., overlapped with another line). These PSLs were also eliminated to avoid printing errors and to reduce material waste.

4. Methodology

As previously mentioned, an advantage of using PSL as a toolpath optimization strategy is that a PSL is formed by a set of nodes grouped in the principal direction with the minimum bending to the structure. Due to the well-defined geometric characteristic, PSL can be quickly calculated and converted to machine instructions (i.e., G-code) using less computational resources, even in domains with a large number of elements. For example, to generate the G-code for a PSL, we need to compute its nodes one-by-one and export the coordinates of the nodes in the format of linear translation commands, such as $G1 Xx Yy Zz Ee$, where x , y , and z are the node positions. The extrusion rate command E is related to the amount of the extruded material that is required and can be calculated using the distance between the nodes. Once a PSL is

converted to toolpath, the closest point along the domain boundary of the next PSL is selected as the first point of the new toolpath being converted. This step is important to reduce the print head travel distance and consequently, the printing time. This process iterates until all the lines are visited.

Although the conversion from PSL to toolpath is straightforward, several research questions need to be addressed. First, how the PSLs should be constructed such that the infill ratio can be controlled? Second, when the PSLs are interlaced, how can they be printed so that the final part's structural integrity is preserved? Third, when the topologically optimized toolpaths are not regular, how to resolve the overlapping of neighboring lines when the lines get close to each other? The following subsections will present our investigation to address these research questions.

4.1. Infill ratio

One attractive feature of AM processes is the capability of fabricating internal voids to minimize part weight. Therefore, the toolpath planning system for AM needs to take the infill ratio as one of the input parameters to control the volume of deposited material and the porosity inside the fabricated part. For the commonly used uniform patterns, the infill ratio can be easily fulfilled by merely scaling the size of the unit cell to match with the material-to-void ratio. In comparison, non-uniform infill patterns, in general, could have better stress redistribution and can achieve better part performance than the uniform ones. However, the principle of controlling the infill ratio used for the uniform patterns does not apply to the non-uniform ones. For example, Steuben et al. [31] introduced a scalar parameter in the implicit function to control the infill ratio, while they did not mention how to set the parameter to achieve a specific infill ratio. Our PSL-based infill pattern is also non-uniform, and the length of each PSL is unknown before computing the PSLs based on given seed points. Fortunately, the PSL computation is very fast, and an iterative search method to find the right PSL density to obtain the desired infill ratio can be developed.

Algorithm 1. Infill Ratio Binary Search

```

1: function INFILL I
2: Require:  $0 < I < 100$ 
3:    $n_l \leftarrow n_{\min}$ ,  $n_r \leftarrow n_{\max}$ ,  $n \leftarrow (n_l + n_r)/2$   $\triangleright$  for search
4:   for  $k = 0$  to  $\text{max\_s teps}$  do
5:      $S \leftarrow \text{GENERATESEEDS } n$   $\triangleright$  Generate seeds uniformly
6:      $\text{PSL} \leftarrow \text{GENERATEPSL } S$   $\triangleright$  Generate PSLs
7:      $i \leftarrow (V(\text{PSL})/V(\text{total})) \times 100$   $\triangleright$  Infill ratio
8:     if  $\text{abs}(I - i) > \text{max\_error}$  then
9:       if  $i < I$  then
10:         $\Delta_{\text{seed}} \leftarrow \text{abs}(n_l - n)/2$ 
11:         $n_l \leftarrow n$ ;
12:         $n \leftarrow n + \Delta_{\text{seed}}$   $\triangleright$  Increase seed count
13:        else
14:           $\Delta_{\text{seed}} \leftarrow \text{abs}(n_r - n)/2$ 
15:           $n_r \leftarrow n$ ;
16:           $n \leftarrow n - \Delta_{\text{seed}}$   $\triangleright$  Decrease seed count
17:        end if
18:      else
19:        return PSL  $\triangleright$  Return PSLs
20:      end if
21:    end for
end function

```

To generate an infill pattern to cover the whole domain, the PSLs are traced from a set of seed points distributed uniformly along the domain boundary. In this way, controlling the number of seed points can change the number of PSLs generated, thus can change the amount of infill in the sliced shape.

Hence the goal is to find the number of seed points necessary to fulfill the requested infill ratio value. Assume there are n seeds $s = \{s_i, i = 1, 2, \dots, n\}$ separated by a distance of $\Delta_d = l/n$, where l is the total length of

the domain boundary. The relationship between the number of seeds and the infill ratio is demonstrated visually in the Symmetric Cantilever domain shown in Fig. 4(a)–(d). Varying the number of seeds from 14 to 75, the obtained infill ratios for this example are 14% to 72.4%. The study on varying seed point numbers was also performed in an L-Shape, an asymmetric cantilever, and bridge test cases (refer to Section 5). The different results were combined and is shown in Fig. 4(e). The plot shows the relationship between the infill ratio and the number of seed points for different domains. It can also be seen that, with the increase in the number of seed points, the infill ratio increases monotonically.

Based on the observation, an iterative optimization procedure is presented in Algorithm 1, in which the desired infill ratio (I) is specified as the input, and the output is a set of PSLs, i.e., $\text{PSL} = \text{Infill}(I)$. The algorithm uses a binary search method, starting from the average value between the maximum and the minimum number of seeds and incrementally increasing or decreasing to get the optimal value. The maximum value, n_{\max} , is the maximum number of seed points that can be generated for a boundary without the lines overlapping. Let the length of a boundary be l and the line width w , then $n_{\max} = l/w$. The minimum number of seed points, n_{\min} , is set to be zero. The parameter max_s teps controls the maximum number of interactions in order to avoid an infinite loop. The end condition is when the difference between the desired infill ratio I and the obtained infill ratio i is smaller than a threshold max_error . In this work, it was considered $\text{max_error} = 5\%$. This algorithm calls two functions: $\text{GENERATESEEDS } (n)$ that generates n seeds uniformly along the outer domain boundary, and then the function $\text{GENERATEPSL}(S)$ to compute the PSLs for the generated seed points as described in Section 3.

4.2. Tension and compression analysis

In traditional slicer software, when the toolpath is generated, there is no concern about how the printing order of paths will affect the component performance. For example, when the infill pattern has interlaced lines, the 3D printer normally prints one direction of the lines first and then prints the lines in the other direction crossing over the previously printed lines. This crossover is usually acceptable as the intersections are small since it is preferred to preserve the structural integrity of the lines than to making stops at each intersection. In most current slicing software, the crossover has been done randomly. However, the order to print the PSLs can be further optimized to enhance the printed object's mechanical properties due to the additional information provided by the stress field. Again, while the FFF process is discussed here, the developed principle and the related procedure can be applied to other AM processes.

In an FFF machine, when two material deposition paths intersect each other in the same layer, the first one will be printed as usual, while the second one will be blocked by the first one, which results in a weaker connection at the intersection point. Although the discontinuous toolpath may not have a significant effect on compressive loads, the discontinuous printed line will decrease the segment strength when tensile loads are applied to it. To avoid this weakening effect for the tensile loads, we should reduce the number of discontinuities as much as possible for the lines that are under tensile load. Due to the given computed stress field, it is possible to classify the PSLs into two different groups: *tensile* and *compressive* PSLs. The classification is obtained using the minimum or maximum principal stress correlated with the principal direction θ_i obtained for each PSL point p_i , as described in Section 3. An intuitive way is to use the local stress values, but it could result in the segments of one PSL being classified into different groups. Printing them separately would introduce unnecessary discontinuities, damage the integrity of the PSL, and weaken the structure. To print the PSLs as continuously as possible, we classify the PSLs as a single unit and not as separate segments. Therefore, the average stress of all the points contained in the PSL is selected in this paper as an approximator for the classification. Therefore, the average stress of all the points contained in

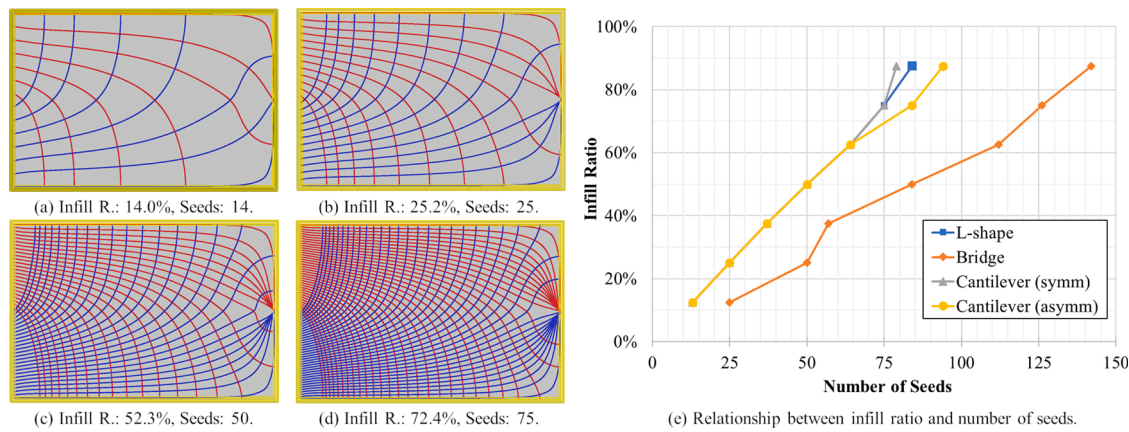


Fig. 4. (a–d) Four different infill ratios for the symmetric cantilever example varying the number of seeds from 14 to 75. (e) The different results combined for the same study considering the in L-shape, bridge, symmetric cantilever, asymmetric cantilever, and bridge domains.

the PSL is further calculated. If the average stress $\sigma_a \geq 0$, the PSL is classified as a compressive PSL; otherwise, it is classified as a tensile PSL. This classification is beneficial in toolpath planning since the printing order of PSLs on the intersection point can be planned to improve the mechanical properties of the 3D printed part.

To generate the final toolpaths with proper printing order, a data structure was created with three groups. Besides the two groups of compressive and tensile PSLs, the third one is the wall group, containing the toolpath for the domain boundary. The order in printing them is firstly the *tensile PSLs*, followed by the *compressive PSLs*, and finally the *Walls*. This configuration allows the printed tensile PSLs to be in continuous lines. Since there are intersections between different groups, the compressive PSLs are less affected by the discontinuities. The wall group is the last one to print to increase the mechanical strength of the bonding between the wall and the infill (PSLs).

To validate the printing order based on the tensile and compressive classification, two types of test specimens with the same infill pattern were fabricated, with one having a random printing order and the other one following the compressive/tensile classification. The two specimens had the same weight and were tested using the same condition (the cantilever case in Fig. 2). For each type of test specimen, three duplicate tests were performed. The maximum loads supported by the test specimens that consider compressive/tensile classification were 37.49, 38.13,

and 39.40 kgf, respectively. The average load is 38.34 kgf. For the test specimens with random printing order, the maximum loads were 32.55, 33.84, and 30.7 kgf, respectively. The average load is 32.39 kgf. Therefore, with the aid of the PSL tensile and compressive classification and the accordingly planned printing order in each PSL line, it was possible to increase the mechanical strength of the test samples by 18.4%

4.3. Extrusion rate

Since the PSLs are generated based on the stress field, they tend to meet and concentrate in the regions with high stresses, especially near constraint points. This agglomeration of material contributes to the redistribution of materials so that the overall performance of the component is enhanced with more materials in the high-stress area. However, when the PSLs are getting too dense, excessive material overlapping between the lines may occur (refer to Fig. 5(a) top). This behavior is similar to other non-uniform infill patterns [31]. The overlapping typically does not create failures in the fabrication process; however, there may be undesired consequences like discontinuous lines due to the blocking by the existing lines or reduced printing quality due to the material scattering. Therefore, the overlapping should be controlled in the toolpath planning to ensure print quality and better use

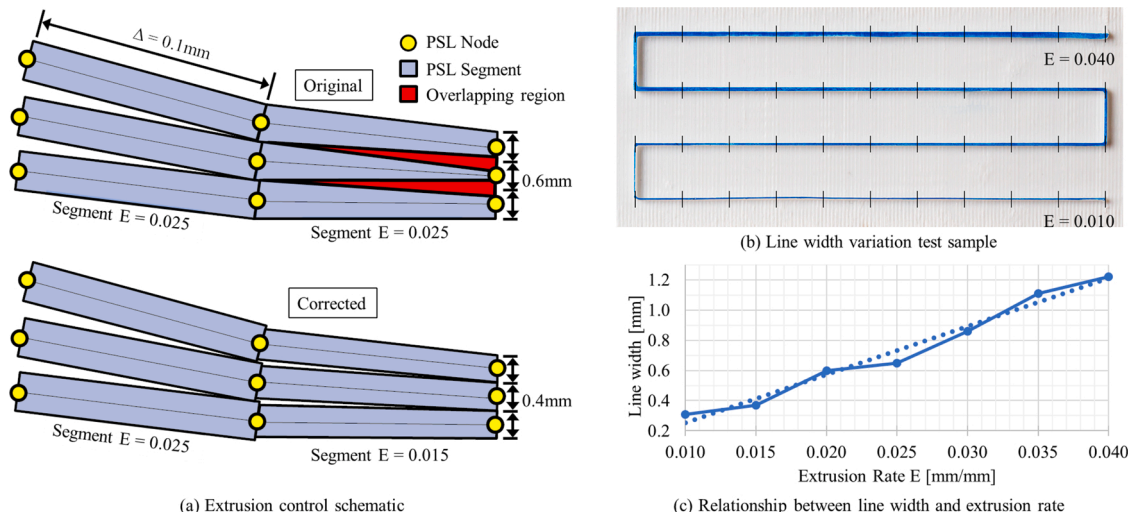


Fig. 5. (a) Top illustrates the segment overlap, shown in red, which can occur. In (a) bottom the overlapping is eliminated with the reduction of the segment extrusion rates E from 0.025 to 0.015 mm/mm. (b) The printed test sample. The blue line has E increased by 0.001 every 10.0 mm. (c) The line width measurements performed on the test sample (solid line), and the trend line (dotted line). (For interpretation of the references to color in this figure legend, the reader is referred to the web version of this article.)

of material. Based on the intrinsic characteristics of PSLs, a possible solution to the line-overlap problem could be a traditional closest point search routine, where a smooth recursive function increases the distance between lines as necessary to avoid the overlap. However, such an approach is computationally expensive and may alter the structural performance as the new line position might not follow the PSL and could be in a low-stress region.

Since the PSL-based toolpath planning is applied in layer slicing, it is possible to solve the toolpath planning problem using material deposition parameter control. Recall that the extruder in an FFF printer is run by a sequence of G1 linear movement commands, e.g., in the form of G1 Xx Yy Zz Ee, where E is the extrusion rate to specify the amount of material (in mm/mm) deposited while moving from one point to another. By manipulating the value of parameter E , it is possible to control the extrusion rate and, consequently, the width of the extruded lines. In other words, the line width can be changed in a path during the printing process. A test sample was printed using an Ultimaker 3D printer is shown in Fig. 5(b) to illustrate the idea. The G-code was created using python so that no geometric slicing was performed to ensure complete control of the printing process. The material used in the test was a white PLA. The layer height was set to 0.2 mm, and the nozzle diameter was 0.4 mm. Blue ink was used to improve line width visualization. A rectangular base 1.0 mm high was used to support the printing. The first 10 printed segments uses a constant value of $E = 0.010$ mm/mm. After the tenth segment, the extruded line was generated increasing the value of E from 0.011 to 0.040 mm/mm with the step size of 0.001 per 10.0 mm. The printed sample is shown in Fig. 5(b). The line width of each segment was measured using a digital caliper. The increase in line width from $E = 0.010$ to the last segment printed with $E = 0.040$ mm/mm can be observed.

The results of the measured line widths are shown in Fig. 5(c), where the horizontal axis is the extrusion rate E , and the vertical axis corresponds to the line width. The line width follows a linear relationship with the extrusion rate. Therefore, a linear equation can be estimated to control the extrusion rate based on a given line width. Accordingly, an algorithm has been developed to allow the reduction of line overlapping. Each PSL is checked with its neighboring PSLs to find if they have any overlapping segments. If there is overlapping, the maximum line width for each node is computed, such that the line segments only touch each other. After that, the new line width is used to calculate the corresponding extrusion rate E at that particular segment. The new E value is associated with the line segment in generating G-code. Therefore, since the E value is individually specified for each line segment, a single toolpath line can have different line widths along its length (see Fig. 5(a) bottom). This method has the advantage of ensuring the lines faithfully follow the principal directions since the line nodes are not moved. Furthermore, it only needs to update the E values during the toolpath generation without introducing additional control parameters. Besides the length of PSLs, the infill ratio calculation can also consider the width of each line segment.

The extrusion rate is adjusted based on the amount of overlap between PSLs. When the number of overlapping PSLs increases, the value of E for each of them is reduced. The relationship between the number of overlapping PSLs (n) and the extrusion rate can be described as $E \propto 1/n$. The present method works well with most cases, and the material can be fused nicely (Fig. 2(f)). However, in an extreme case, when a region has many overlapping PSLs ($n \rightarrow \infty$), the extrusion rate will be too small ($E \rightarrow 0$) that no material will be added to the region. To avoid such overcompensation, several PSLs are randomly selected to print with the minimum extrusion rate (i.e., $E_{\min} = 0.01$ mm/mm in this paper) when a region has too many overlapping PSLs.

5. Results

The proposed framework was implemented with VC++ and numerically tested with physical experiments. The testing results are

presented in this section. As mentioned in Section 3, most AM processes fabricate parts layer-by-layer, and the toolpath planning in 2D layers is critical no matter how the 3D shape is optimized in the CAD phase. Therefore, this work focuses on the toolpath generation on a 2D plane with a given 2D stress field. All the tests were run on a computer with Intel Core I7-3770K @ 3.50 GHz, 32 GB of RAM, and Windows 7 64bits. In the study, the PSL infills were compared with other infills. The presented method was applied in various design cases, and the time statistics were recorded and reported in the section.

5.1. Comparison with other infills

The cantilever problem was studied to verify the PSL-based toolpath planning method in enhancing part strength (Fig. 2). In this example, a 2D rectangular domain was employed, in which the fixed boundary conditions were applied at one end, and a load was applied in the middle of the other end. The related stress field is visualized in Fig. 2(c). The high-stress areas are located near the constraints and the load, indicated by the red color. The toolpath visualization in Fig. 2(d) indicates that all the infill toolpaths generated in the upper part of the domain are in the tensile group (red), while the bottom ones are in the compressive group (blue). This stress analysis result indicates that the PSL classification worked as expected since the downward load will generate compressive and tensile stresses on the bottom and the top of the domain, respectively.

Three other uniform infills that are commonly used were created using an open-source 3D printer slicing application – Cura. They are Triangle, Tri-hexagon, and Grid (Fig. 6). The infill ratio for all the cases was set to 45% in Cura. They were used to compare with our PSL-based toolpath fabrication results.

Firstly, all the four infill patterns were compared numerically using the finite-element method and the fracture analysis. A finite element model was created for each infill with one single layer using exclusively beam elements. The boundary conditions applied were the same, as shown in Fig. 2(a). All the models had the same amount of deposited material. The walls have a width of 1.2 mm, and the infill line width is 0.4 mm.

Physical destructive tests were also performed on the fabricated samples. All the test samples were printed by using an Ultimaker 3 FFF 3D printer with the same material batch. The selected material was silver polylactic acid (PLA). The layer thickness used in fabrication was 0.20 mm, and the test specimens dimensions were 40 mm × 60 mm × 5 mm. The top and bottom surfaces were disabled to allow easy visualization of the infill patterns and the failure mode. The samples were weighed to confirm that they had the same amount of material. The fabricated test specimens are shown in Fig. 6(a)–(d). The experiments were performed using a Mark-10 tensile tester machine, as shown in Fig. 6(e). The force was measured by a load cell connected to the data acquisition system. All the tests were realized under the same boundary conditions and external load. The tests were performed until the complete fracture of the samples, as shown in Fig. 7.

For each test specimen (PSL, Grid, Triangle, and Tri-Hexagon), three identical tests were performed (samples #1, #2, and #3) following the same procedure described in this section. All the uniform infills were broken by the edge along with the boundary conditions, while the PSL infill was fractured around the center. These results corroborate with the numerical simulation in Fig. 8. The result values reported in Table 1 are the maximum load sustained by each of the test specimens. As can be observed, the test specimen with the PSL-based infill has the best result by supporting a force of 38.34 kgf, an increase of 54.6% when compared with the Triangle infill. It is important to note that the only difference between the PSL and the other three test specimens is that different infill patterns were utilized in the layer-based deposition process.

Numerical simulation and fatigue analysis were also done to understand the pattern difference better. Nastran, with solution 101, was used to find the stresses. During the iterations, elements with high

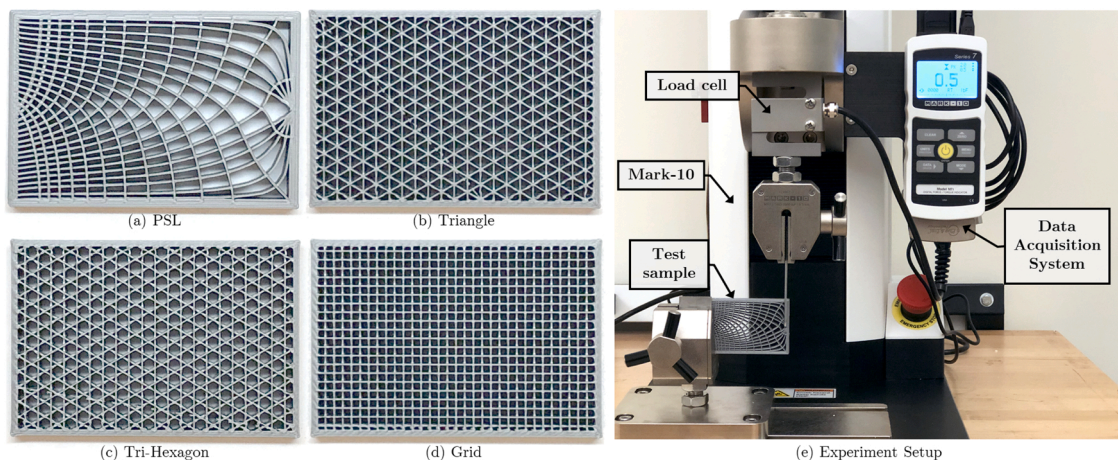


Fig. 6. Physical test and comparison of different infill patterns. (a) The proposed PSL pattern considering the given design requirement, and (b)–(d) are the uniform patterns created by commercial software. All samples have the same mass and were printed with the same material using the same FFF machine. (e) The physical experimental setting for the destructive tests.

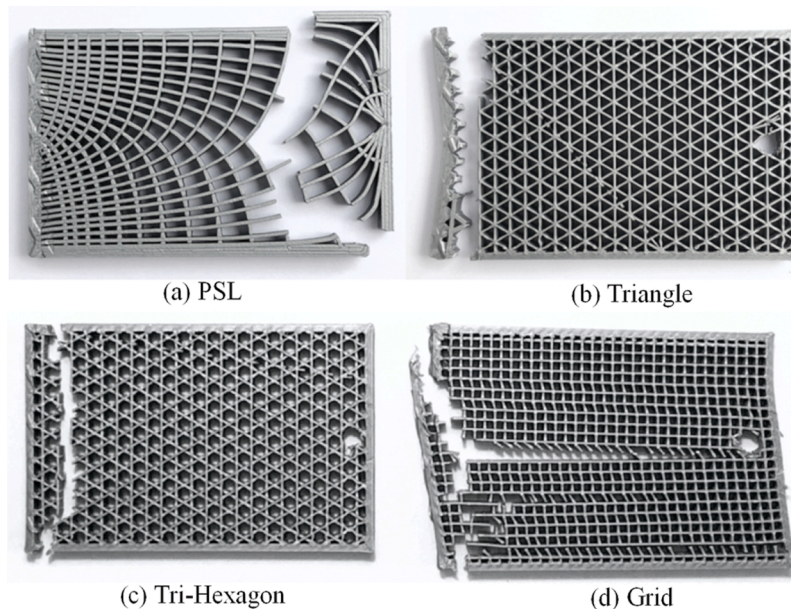


Fig. 7. Photography of the test samples, shown in Fig. 6(a)–(d), after the tests.

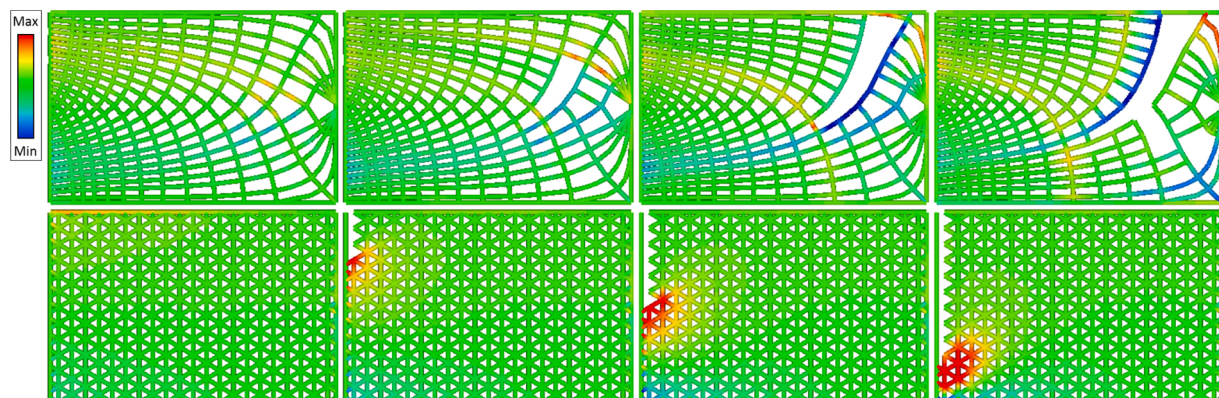


Fig. 8. Finite element and fracture analysis comparison between the PSL and the Triangle infills. The color maps show the maximum principal stresses. Stresses higher than the material tensile ultimate stress are shown in red. The PSL infill shows a stress redistribution during the fracture, while the triangle infill has high-stress concentration along the left boundary. (For interpretation of the references to color in this figure citation, the reader is referred to the web version of this article).

Table 1

Results from the testing between different infills (values in kgf).

Sample	PSL	Grid	Triangles	Tri-Hexa
#1	37.49	26.22	24.88	25.87
#2	38.13	25.85	25.36	26.97
#3	39.40	25.18	24.13	24.95
Average	38.34	25.75	24.79	25.93

compressive or tensile stress ($\sigma > 27$ MPa) were removed from the model to simulate the fracture growth. The results are shown in Fig. 8, in which only the Triangle pattern is shown as a representative of the uniform infills. The Tri-Hexagon and the Grid had the fracture results that are very similar to the Triangle pattern with the fracture occurring in the same way and the same region. For the uniform infills, the fracture always occurs in the region near the constraints, where the highest stresses concentrate on this cantilever configuration. The fracture keeps propagating, from top to bottom, around the high-stress region along a straight line. Unlike the uniform infill, the PSL-based infill had a more uniform stress distribution, and the fracture starts from a line around the middle point of the domain rather than around the boundary conditions. The fracture propagates in a curved shape following the PSL direction until it reaches the domain boundary. These results demonstrate that the PSL infill can pass the stresses from the highly concentrated regions to other regions, and redistribute the stresses when a fracture occurs, allowing better structural performance.

5.2. Other examples

The proposed method was also tested by using various boundary conditions, as shown in Fig. 9. For each of the infill domain, a stress field was computed in 2D by the given loads. Using the framework, the PSLs were then generated with a target infill around 50%. The generated PSLs were converted to toolpath with the wall lines created. Different toolpath groups are differentiated by the colors shown in the last column of Fig. 9. The yellow lines indicate the wall group; the red ones indicate the toolpath of the tensile group, and the blue ones indicate the toolpath belonging to the compressive group.

The first row in Fig. 9 is an asymmetric cantilever problem with the downward load at the bottom-right corner of the infill domain. The stress field shows that it can account for the difference in stress distribution compared with the symmetric case. The toolpaths generated by

our method conform well with the results presented by the 3D infill optimization method [10], but with a higher resolution. It can also be seen that the proposed framework can work for both symmetric and asymmetric cases without modifying the method.

The second example in Fig. 9 is a typical bridge case with one constraint in each of the lowest corner of the infill domain. The load was applied in the horizontal center at the bottom of the domain. The constraint and load regions presented the highest stresses. The compressive PSLs form arcs to connect the supports, while the tensile PSLs connect the compressive lines to the point of load.

We have also tested our framework examining the symmetric cantilever problem with an out-of-plane load. The result is shown in Fig. 10. The beam thickness is 5 mm, and different layer thicknesses were selected, as shown in the first row of the figure. The height of the top surface $H = 5.0$ mm, and the bottom surface $H = 0.0$ mm. The neutral plane is located at $H = 2.5$ mm. The 3D strain field was sliced into multiple 2D layers with a layer thickness of $h = 0.25$ mm. The toolpaths were generated for each 2D strain field. The bottom layer $H = 0.0$ mm is under compressive stresses, and the horizontal PSLs are classified as compressive (blue). At $H = 2.5$ mm, the neutral plane, the PSLs are concentrated near the point where the load is applied. It can be seen in the second row that the stress is near 0 in the neutral plane. At layer $H = 2.75$ mm, just above the neutral plane, the stress becomes larger, and the PSL lines were more defined when compared with the PSLs in the neutral plane. The top layer $H = 5.0$ mm is under tensile stresses, and the horizontal PSLs are classified as tensile (red). As expected, both the top and bottom layers have similar results.

More complex examples were also studied. Fig. 11(a) shows a piston connection rod. Used inside a combustion engine to connect the piston to the crankshaft. One of its primary functions is to transfer the downward load, which occurs on the top surface of the piston during the combustion stroke, translating the linear motion into rotational motion. Suppose a downward load was applied on the interface region between the connection rod base and the piston pin, indicated by red arrows in Fig. 11(b). The bottom region was constrained, simulating the contact with the crankshaft. The CAD model was exported, along with the computed stress field based on the design function. The PSLs were created within the infill domain based on the given stress field, as well as the outer and inner walls, which were converted into toolpaths, as shown in Fig. 11(d). The toolpaths are well distributed, with vertical and horizontal lines to support the axial loads, like a uniform grid, but distorted to conform to the shape of the rod.

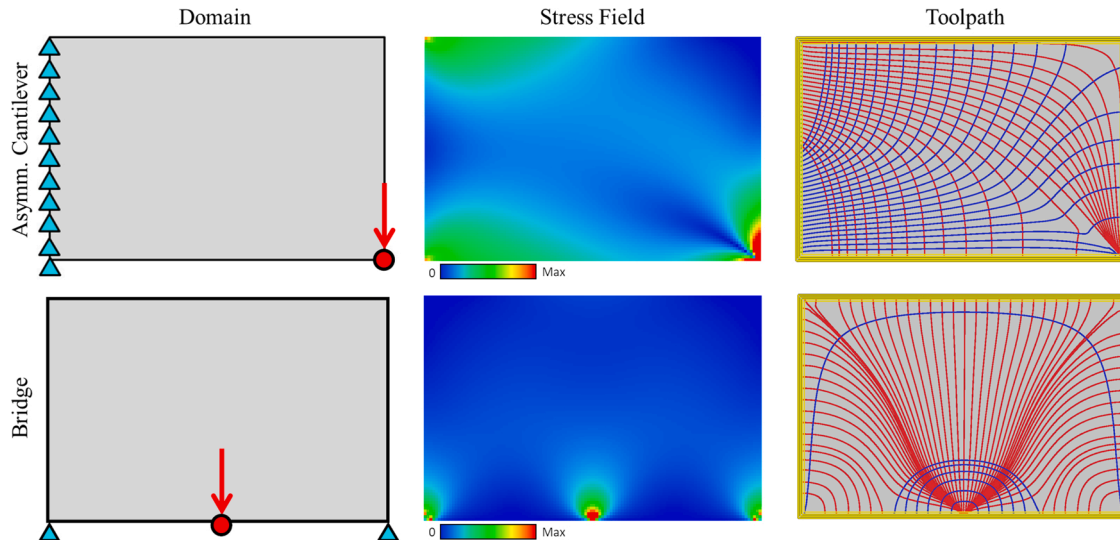


Fig. 9. Asymmetric cantilever and bridge examples. The first column shows the initial infill domain containing the boundary conditions and loads; the second column shows the stress field, and the last column shows the generated toolpaths. (For interpretation of the references to color in this figure citation, the reader is referred to the web version of this article.)

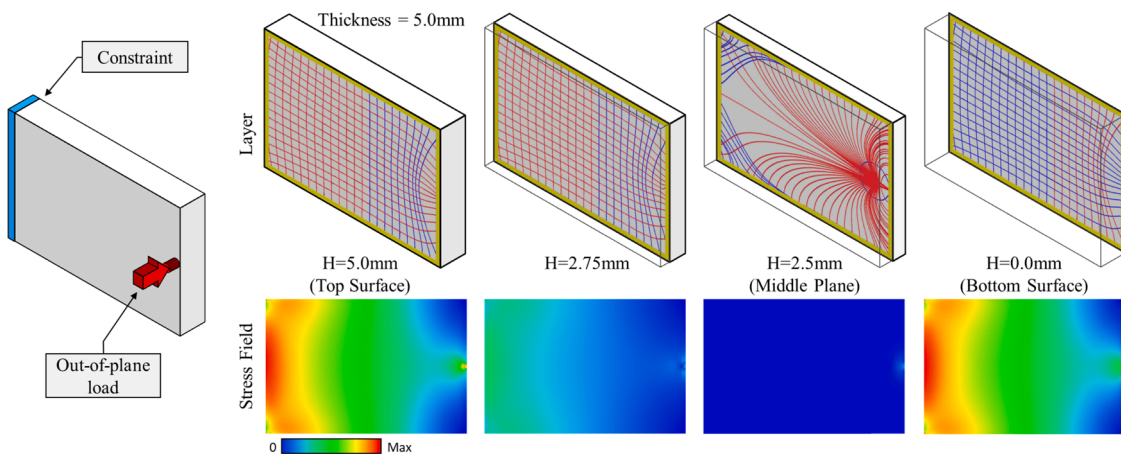


Fig. 10. Example with the out-of-plane load. The top row shows the layer position with the PSL-based toolpath. The wall is shown in yellow, the tensile lines in red, and the compressive ones in blue. The second row shows the equivalent stress field. (For interpretation of the references to color in this figure legend, the reader is referred to the web version of this article.)

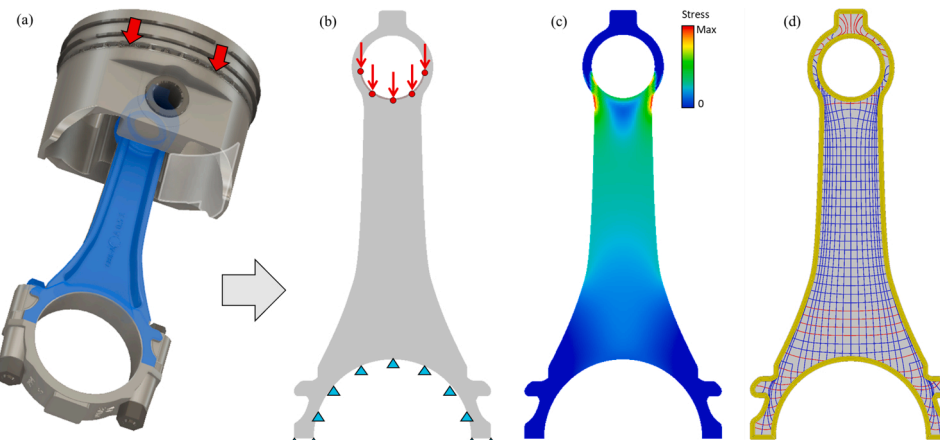


Fig. 11. Example of a piston connection rod. (a) A 3D model of a piston assembly with the connection rod shown in blue. (b) The domain with boundary conditions and loads. (c) The 2D stress field. (d) The toolpaths based on PSL. (For interpretation of the references to color in this figure legend, the reader is referred to the web version of this article.)

Another example in Fig. 12 shows the results for a typical 17 mm

wrench tool. The same procedure shown in the previous examples was used. The strain field was created using a CAD/CAE software system and exported to our framework. The model was sliced based on the stress field, and the toolpath was generated accordingly. The stress field in Fig. 12(b) shows four regions with high-stress concentrations (shown in red). To improve mechanical performance, these regions should have more deposited materials. Fig. 12(c) shows the final toolpaths generated by our method, which successfully fills the high-stress regions with more material following the principal stress directions.

5.3. Time statistics

Since a 3D model can have a large number of layers, the time required to generate the PSLs per layer is important for the practical use of non-uniform infill patterns. Table 2 shows the computational time for different test cases. The column t_{total} contains the time necessary to perform all infill interactions to obtain the desired infill, t_1 shows the time to calculate all PSLs for one layer. The t_1 is depending on the PSL step size Δ as well as the desired infill ratio. Higher infill values tend to demand a higher number of seeds. Therefore, the computation time will increase. In the symmetric cantilever problem, the time spent to generate PSLs with 50 seeds was 0.221 s. Increasing the infill ratio to 75%, 75 seeds were needed to obtain the required infill toolpaths. Consequently, the time increased to 0.383 s. These results show that the

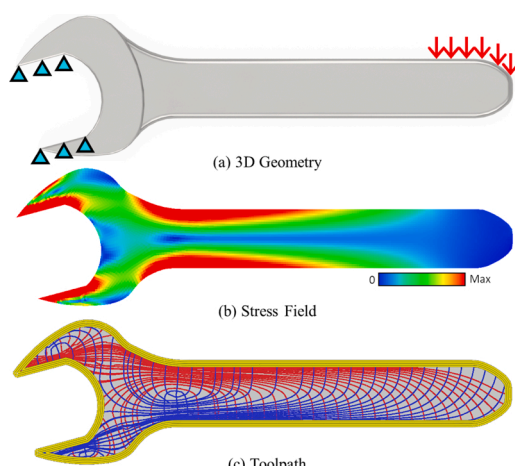


Fig. 12. Wrench example. (a) 3D geometry with boundary conditions and loads. (b) The 2D stress field. (c) The toolpaths based on PSL. (For interpretation of the references to color in this figure citation, the reader is referred to the web version of this article.)

Table 2

Time statistics for the PSL-based toolpath planning. #Ele is the number of elements in the domain, t_{total} is the total time with the binary search, and t_1 is the time for one iteration.

Domain	#Ele	t_{total} [s]	t_1 [s]
Bridge	9600	1.283	0.272
Cantilever (sym.)	9600	0.221	0.221
Cantilever (asymmm.)	9600	0.963	0.290
Piston connection rod	16751	2.661	0.608
Wrench	11482	4.372	0.229

PSL-based toolpath planning method can be reasonably fast for hundreds or even thousands of 2D layers.

This work is a combination of line-based topology optimization and toolpath planning. The time-consuming step in the method is the TO. In comparison, most existing toolpath planning methods are very fast. Hence their time statistics are not reported in this paper. To compare the PSL-based results with other TO methods, the MATLAB codes from Bendsøe and Kikuchi [20] were used to run the SIMP method, and the codes from Wei et al. [19] were used to run the Level-Set method. The selected test case was asymmetric cantilever. The mesh size for all the methods was 120×80 , and the infill ratio is 50%. The convergence time is 1466 s for the Level-Set method, 37 s for the SIMP method, and 0.963 s for our PSL-based method. In addition, the time statistics reported for the Level-Set and SIMP methods only considered the optimization time. The extra time that is necessary to convert the TO results to toolpath was not included. This comparison result shows that our PSL-based method is more efficient and effective, which is important for AM toolpath planning.

6. Discussion

In this section, we will discuss possible variations of the presented method, and present their advantages and disadvantages. The performance and limitations of the presented method under different situations will also be discussed.

6.1. Influence of wall

We studied the influence of the group *Walls* in the PSL generation during the development of this work. Different weighting to the wall was considered during the analysis to simulate a higher perimeter stiffness when compared with the domain's interior. The wall thickness was increased in incremental steps to increase the perimeter stiffness. The thicker the wall, the stronger the perimeter is (Fig. 13(a)).

Fig. 13(b)–(e) shows a symmetric cantilever study. It demonstrates how the additional wall thickness of the perimeter influences the PSLs. It can be seen that even up to a ratio of 7 between the perimeter and the interior, the lines generated are distributed only with slight differences, while the overall shapes are similar. Suppose the border stiffness was much larger than the interior stiffness (like different materials). In that case there could be a significant difference, which needs more study to understand how the ratio should be set for different materials. In our study, we assumed that the whole infill domain has the same weight.

6.2. Extension to more general cases

The contributions of this paper come from solving the toolpath-planning and fabrication related issues in the application of PSL to structurally optimize the 2D sliced layers for 3D printing. In Section 5.2,

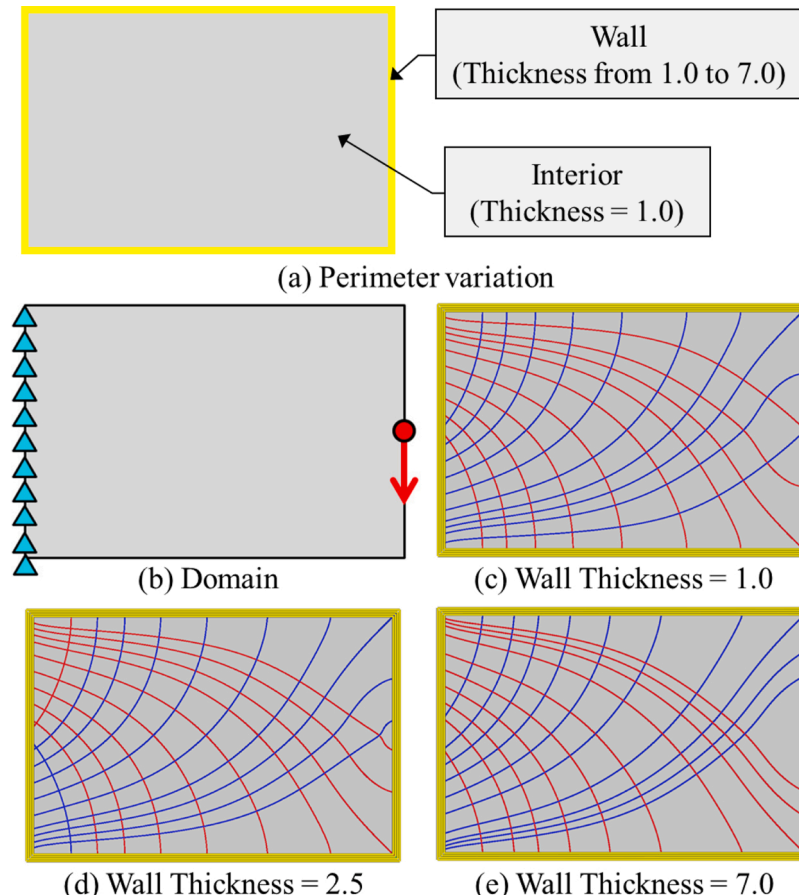


Fig. 13. Example of different weight for perimeters.

a cantilever problem was presented with an out-of-plane load applied. The results demonstrated how our algorithm behaves when a 3D strain field is sliced, and the obtained 2D strain fields differ in each sliced layer. When the principal stress directions are aligned in-plane, the field across different layers should be small. In this case, it just needs to make sure the seed points at a layer are located on top of the ones in the previous layer so that the PSLs will not be offset. However, when the field is discontinued across layers, the PSLs in neighboring layers may go in different directions and become unaligned. Here, fabrication's success is less of a concern because even if a PSL is not supported directly by a parallel one, it will be supported by the perpendicular ones through bridging. Therefore, it is more of a concern on how the stresses are distributed across layers. To consider inter-layer relationships (like compression or tension between layers) by using 2D infills, we can control the local density to put more material in the high-stress areas. This can be done by applying an adaptive sampling of seeds throughout the domain, but it will need certain modeling to define the relationship between stress values and sampling, as the design of the new sampling methodology, which requires more studies and will be one of the future works.

6.3. Selection of sampling method

Based on our study, PSL-based toolpath planning shows quite promising results and need to be further studied. Despite the promising results using uniform seed sampling, different seed sampling methods could be considered. The motivation is to increase the number of seed points that generate PSLs whose trajectory adds material to an objective region. For example, in the cantilever problem, it is interesting to add more material in the region near the constraints, since this region will have the highest stress. Therefore, when an explicit control on the local density is preferred, it can be done by controlling the sampling on the boundary or even directly adding samples inside the infill domain. Due to the fast response of PSL generation, users can directly specify sample points on the boundary and evaluate the results. Fig. 14 shows two options for non-uniform seed sampling. In other possible scenarios, sample points would be added inside the domain to create arbitrary density [42]. An illustration is shown in Fig. 15 with an interior sample point example. A new PSL (red) is created from a new seed point (yellow) at a distance d apart from the previous PSL (green). However, since there will be many more degrees of freedom inside the domain, more studies are needed to design a new sampling method together with the need to not create vulnerable points in the infill pattern.

7. Conclusion

This work demonstrates a new toolpath planning method by considering both design function and manufacturing requirements on material extrusion. The presented method uses a line-based topology

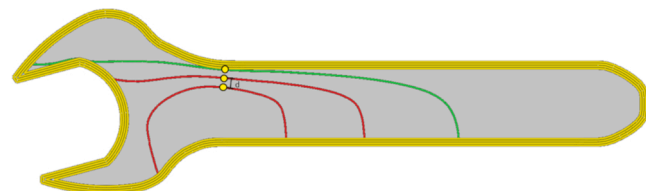


Fig. 15. Illustration of an evenly spaced PSL. (For interpretation of the references to color in this figure citation, the reader is referred to the web version of this article.)

optimization approach so that the computed results can be readily converted into toolpath for 2D layer fabrication. The tested results demonstrated the influence of the optimized toolpath in improving the mechanical strength of the fabricated components. In our developed method, a strain field is given, and an optimized toolpath can be computed using the principal stress lines (PSL). The use of the PSL-based optimization method is fast, reliable, and able to generate toolpaths that conform to given design requirements. The experimental results show a significant increase in mechanical strength when compared with other regular infill patterns generated by commercial software. The tested component with our optimized toolpaths was 54.6% stronger in the ultimate load. The non-uniform infill based on PSLs can also redistribute the stresses. To control the infill ratio in a non-uniform pattern, a binary-search algorithm was developed to obtain the desired infill density. If the infill ratio is very high, for example, 100%, a hybrid infill may be used, in which empty areas are filled with regular infill types. Using the stress field, PSLs can be classified as compressive or tensile. The classification allows further optimization of the printing order, and the tensile lines are printed first to avoid discontinuities that weaken the tensile strength. PSL classification increased the part mechanical strength by 16.4%, when compared with a test sample without such classification. To reduce material overlapping, a method of adjusting process parameters for the toolpath planning was developed. By controlling the amount of extruded material, it was possible to vary the line width of a toolpath. A study was performed to obtain the relationship between the extrusion rate E and the line width.

There are some future works to be performed. In the current implementation, our framework considers a 3D model as the stacking of multiples 2D layers, and only the individual 2D slices were planned based on PSLs. Further work is necessary to extend the method to address 3D loading cases. For example, while planning toolpaths of a layer, the previous and next layers need to be taken into account so that the printing can increase the inter-layer strength. Our current method was demonstrated mainly for the FFF process. This study can also be extended to different line-based AM methods, such as direct energy deposition (DED) and selective laser melting (SLM). There are similarities and differences between FFF, DED, and SLM. While FFF

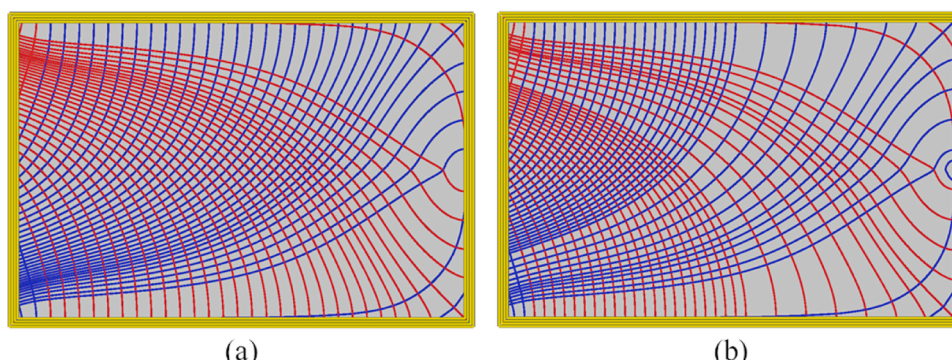


Fig. 14. Different non-uniform examples for the symmetric cantilever example. (a) Non-uniform sampling, the left, top, and bottom regions have twice the seed density than the right region. (b) Non-uniform sampling, the left region, close to the constraint, has twice the seed density than the right region.

accumulates material by melting a continuous thermoplastic filament using a heated nozzle and depositing it line-by-line, DED and SLM use a high-energy laser beam to melt and fuse the metal material in a powder bed. On the one hand, since the AM methods all use a motion controller to direct the material addition, the toolpath and the computational code (i.e., G-code) to perform such operations still need to be obtained. On the other hand, they have different process parameters and characteristics, e.g., FFF deposes the melt material on the completely solidified material, but SLM also partially re-melts the previously joined material. In this paper, the proof-of-concept was done with the FFF printer. Hence the toolpath was optimized with the line continuity and extrusion rate of the FFF process. The same principle would be applied with DED and SLM with the parameters like laser intensity and scanning speed to produce an optimized toolpath considering the DED and SLM characteristics, which requires further study and will be investigated in our future work.

Declaration of Competing Interest

The authors report no declarations of interest.

Acknowledgment

This paper acknowledges the support of the Natural Sciences & Engineering Research Council of Canada (NSERC) grant #RGPIN-2017-06707, and the National Science Foundation (NSF) CMMI 1663663.

Conflict of interest: None declared.

References

- [1] Gao W, Zhang Y, Ramanujan D, Ramani K, Chen Y, Williams CB, et al. The status, challenges, and future of additive manufacturing in engineering. *Comput-Aided Des* 2015;69:65–89.
- [2] Bourell DL. Perspectives on additive manufacturing. *Annu Rev Mater Res* 2016;46: 1–18.
- [3] Alani T, Othman F, Ali H. Effect of infill parameter on compression property in fdm process. *Int J Eng Res Appl* 2017;7:2248–962216.
- [4] Alvarez K, Lagos R, Aizpuri M. Investigating the influence of infill percentage on the mechanical properties of fused deposition modelled abs parts. *Ing Investig* 2016;36:110–6.
- [5] Lu L, Chen B, Sharf A, Zhao H, Wei Y, Fan Q, et al. Build-to-last: strength to weight 3d printed objects. *ACM Trans Graph* 2014;33:1–10.
- [6] Wang TY, Liu Y, Liu X, Yang Z, Yan D, Liu L. Global stiffness structural optimization for 3d printing under unknown loads. *J Comput Graph Technol* 2016;5:18–38.
- [7] Ahn S-H, Roundy And S, Wright PK, Montero M, Odell D, Roundy S. Anisotropic material properties of fused deposition modeling abs. *Rapid Prototyp J* 2002;8.
- [8] Rankouhi B, Javadpour S, Delfanian F, Letcher T. Failure analysis and mechanical characterization of 3d printed abs with respect to layer thickness and orientation. *J Fail Anal Prev* 2016;16.
- [9] Leung Y, Kwok T-H, Li X, Yang Y, Wang CCL, Chen Y. Challenges and status on design and computation for emerging additive manufacturing technologies. *J Comput Inform Sci Eng* 2019;19.
- [10] Wu J, Aage N, Westermann R, Sigmund O. Infill optimization for additive manufacturing – approaching bone-like porous structures. *IEEE Trans Visual Comput Graph* 2018;24:1127–40.
- [11] Haslinger J, Mäkinen R. Introduction to shape optimization – theory, approximation, and computation. Society for Industrial and Applied Mathematics; 2003.
- [12] Bendsoe M, Sigmund O. Topology optimization: theory, methods and applications. Berlin: Springer; 2003.
- [13] Dapogny C, Estevez R, Faure A, Michailidis G. Shape and topology optimization considering anisotropic features induced by additive manufacturing processes. *Comput Methods Appl Mech Eng* 2019;344:626–65.
- [14] Mirzendehe AM, Rankouhi B, Suresh K. Strength-based topology optimization for anisotropic parts. *Addit Manuf* 2018;19:104–13.
- [15] Osher S, Sethian JA. Fronts propagating with curvature-dependent speed: algorithms based on Hamilton-Jacobi formulations. *J Comput Phys* 1988;79: 12–49.
- [16] Allaire G, Jouve F. Minimum stress optimal design with the level set method. *Eng Anal Bound Elem* 2008;32:909–18. Shape and Topological Sensitivity Analysis: Theory and Applications.
- [17] Suresh K, Takalloozadeh M. Stress-constrained topology optimization: a topological level-set approach. *Struct Multidisc Optim* 2013;48:295–309.
- [18] Xia Q, Shi T, Liu S, Wang MY. A level set solution to the stress-based structural shape and topology optimization. *Comput Struct* 2012;90–91:55–64.
- [19] Wei P, Li Z, Li X, Wang MY. An 88-line matlab code for the parameterized level set method based topology optimization using radial basis functions. *Struct Multidisc Optim* 2018;58:831–49.
- [20] Bendsøe MP, Kikuchi N. Generating optimal topologies in structural design using a homogenization method. *Comput Methods Appl Mech Eng* 1988;71:197–224.
- [21] Rozvany GIN. A critical review of established methods of structural topology optimization. *Struct Multidisc Optim* 2009;37:217–37.
- [22] Dorn W. Automatic design of optimal structures. *J Mecanique* 1964;3:25–52.
- [23] Hagishita T, Ohsaki M. Topology optimization of trusses by growing ground structure method. *Struct Multidisc Optim* 2009;37:377–93.
- [24] Zegard T, Paulino GH. Grand – ground structure based topology optimization for arbitrary 2d domains using matlab. *Struct Multidisc Optim* 2014;50:861–82.
- [25] Alzahrani M, Choi S-K, Rosen DW. Design of truss-like cellular structures using relative density mapping method. *Mater Des* 2015;85:349–60.
- [26] Zhang P, Toman J, Yu Y, Biyikli E, Kirca M, Chmielus M, et al. Efficient design-optimization of variable-density hexagonal cellular structure by additive manufacturing: theory and validation. *J Manuf Sci Eng* 2015;137. 021004-021004-8.
- [27] Ezair B, Fuhrmann S, Elber G. Volumetric covering print-paths for additive manufacturing of 3d models. *Comput-Aided Des* 2018;100:1–13.
- [28] Jin Y, Du J, He Y, Fu G. Modeling and process planning for curved layer fused deposition. *Int J Adv Manuf Technol* 2017;91:273–85.
- [29] Wu J, Wang CC, Zhang X, Westermann R. Self-supporting rhombic infill structures for additive manufacturing. *Comput-Aided Des* 2016;80:32–42.
- [30] Liu J, Ma Y, Qureshi AJ, Ahmad R. Light-weight shape and topology optimization with hybrid deposition path planning for fdm parts. *Int J Adv Manuf Technol* 2018; 97:1123–35.
- [31] Steuben JC, Iliopoulos AP, Michopoulos JG. Implicit slicing for functionally tailored additive manufacturing. *Comput-Aided Des* 2016;77:107–19.
- [32] Michell AGM. The limits of economy of material in frame-structures. *Lond Edinb Dublin Philos Mag J Sci* 1904;8:589–97.
- [33] Bellini A, Gücüri S. Mechanical characterization of parts fabricated using fused deposition modeling. *Rapid Prototyp J* 2003;9:252–64.
- [34] Zhang P, Liu J, To AC. Role of anisotropic properties on topology optimization of manufactured load bearing structures. *Scr Mater* 2017;135:148–52.
- [35] Koch C, Hulle LV, Rudolph N. Investigation of mechanical anisotropy of the fused filament fabrication process via customized tool path generation. *Addit Manuf* 2017;16:138–45.
- [36] Wittbrodt B, Pearce JM. The effects of pla color on material properties of 3-d printed components. *Addit Manuf* 2015;8:110–6.
- [37] Daynes S, Feih S, Lu WF, Wei J. Optimisation of functionally graded lattice structures using isostatic lines. *Mater Des* 2017;127:215–23.
- [38] Gao G, Liu Z, Li Y, Qiao Y. A new method to generate the ground structure in truss topology optimization. *Eng Optim* 2017;49:235–51.
- [39] Tam K-MM, Mueller CT. Additive manufacturing along principal stress lines. *3D Printing Addit Manuf* 2017;4:63–81.
- [40] Kwok T-H, Li Y, Chen Y. A structural topology design method based on principal stress line. *Comput-Aided Des* 2016;80:19–31.
- [41] Andreassen E, Clausen A, Schevenels M, Lazarov BS, Sigmund O. Efficient topology optimization in matlab using 88 lines of code. *Struct Multidisc Optim* 2011;43: 1–16.
- [42] Jobard B, Lefer W. Creating evenly-spaced streamlines of arbitrary density. *Visualization in scientific computing* 97. Springer; 1997. p. 43–55.